DIELECTRIC RESONATOR OSCILLATORS

Oscillators producing energy at microwave frequencies are an essential component in most microwave communication systems, such as communication links, radar, frequency synthesizers, and so on. There are significant commercial pressures to improve the performance of oscillators with respect to giving them lower noise characteristics, higher dc to RF efficiency, better temperature and frequency stability, etc. The dielectric resonator when coupled with two or three terminal active devices provides a vehicle for producing high quality fixed frequency or narrowband tunable oscillators. Low loss temperature stable dielectric materials with high quality Q-factors mean that miniature resonators can be formed which have physical compatibility with microwave integrated circuits (1). A dielectric resonator (DR) can be used to form the stabilizing element in an oscillator. Dielectric resonator oscillators (DROs) are characterized by the following properties: high frequency stability, high efficiency, and low manufacturing cost. They also can be made to provide good temperature stability.

Two and three terminal active devices exhibit phase noise characteristics at microwave frequencies. Oscillators constructed using these devices can have their phase noise behavior improved by the addition of a DR element.

For a three terminal device the dielectric resonator for first order feedback topologies (2) can occupy one of several positions within the circuit, as illustrated in Fig. 1.

In Fig. 1(a) the DR is mounted in order to provide parallel feedback to the three-terminal active device. Here the coupling action is between device ports (3).

In Fig. 1(b) the DR is located so that energy produced as a result of negative resistance obtained at the device port is reflected back with correct phasing into the active device by the DR, which presents a high impedance at the device port. The DR acts as a bandstop filter, and in this way an oscillation is set up. This configuration has good phase noise characteristics. However, it is sensitive to load variation and tends to mode jump due to the presence of two resonant circuits (4). The configuration in Fig. 1(c) generally provides superior performance to the other two methods and is compatible with the off-chip bonding processes required for stabilizing monolithic microwave integrated circuit (MMIC) oscillators. Here the DR acts as a very high Q resonator element for the series feedback oscillator giving good frequency stability and low phase noise. In a field effect transistor (FET) realization, where the DR is coupled to the gate circuit and the feedback is common source, the operating point is very insensitive to load variation due to intrinsic isolation between the input and output provided by the low gate to drain capacitance of the active device. A varactor diode can be added for tuning purposes. Higher order feedback implementations (5), for example, shunt feedback DRO configurations such as those given in Fig. 2, are also possible (6). Multiple DR and push-push frequency doubling oscillator configurations are also possible (7).

In Fig. 2 the DR behaves as a high Q filter in the positive feedback path. In Fig. 2(a) part of the output signal is coupled back to the input port. By adjusting lengths ℓ_1 and ℓ_2 the Barkhausen oscillation condition can be satisfied. In Fig. 2(b) the DR is coupled between two ports and the output is taken from the third. Here the position of the DR is adjusted in order to maximize the negative resistance at the output port of the active device.

In the shunt feedback configurations the two coupling coefficients in the parallel feedback case cannot be adjusted separately. Also, since the coupling is to an open circuit line these types of circuits tend to be very sensitive to the lateral position of the DR.

The selection of the active device for oscillator applications depends on the frequency of operation. Below 12 GHz, bipolar junction transistors (BJTs) and HBT find application due to their superior flicker, $1/f$, and noise levels (8). In (9) a 4 GHz, 21 dBm series feedback bipolar transistor DR oscillator with a phase noise spectral density of -130 dBc/Hz at 10 kHz from the carrier was reported. Values of -89 dBc/Hz at 10

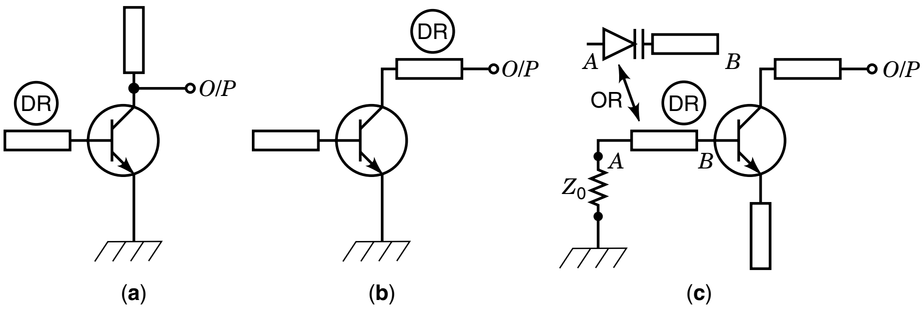

Figure 1. Typical DRO topologies.

kHz offset have been reported at 21.4 GHz for a reflection type DRO producing 10 dBm output power (10). Stabilized Gunn oscillators operating at 35 GHz (11) and HBT DROs at 25 GHz have also been reported (12).

It is significant to note that generally as frequency increases output power can be maintained only at the expense of increased phase noise, since the DR must be coupled more tightly to the circuit.

The key elements to be optimized with respect to oscillator performance are:

- Output power
- Start-up stability
- Phase noise
- DC-RF efficiency
- Tuning range
- Sensitivity to DR placement
- Frequency pushing/pulling

For a very high frequency operation into the millimeter wave region, or for very high Q-factor operation in the centimeter wavelength region, DRs operated in whispering gallery mode (13) are employed (14–16). Here the important dimension is the circumference rather than the diameter of the DR. This leads to more practical sized DRs for higher frequency circuits.

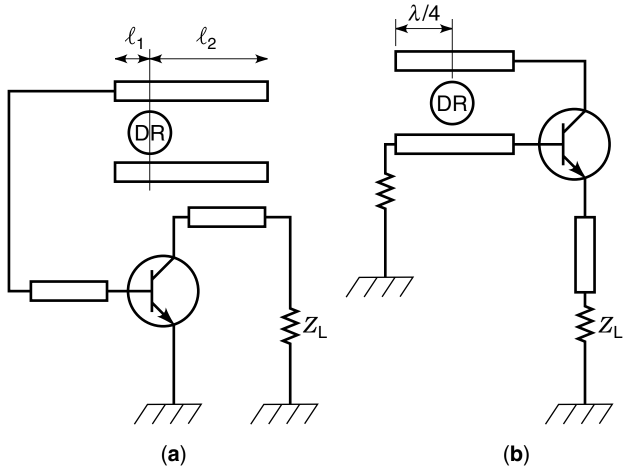

Figure 2. Shunt feedback topologies.

DIELECTRIC RESONATORS

A dielectric resonator (DR) is a high dielectric constant ceramic material formed into a regular geometric shape, usually a solid or hollow cylindrical or cuboid shape. The material usually has a relative dielectric constant of around 30 to 40 (but can be as high as 92) and exhibits low loss characteristics. The high permittivity of the material means that energy can be stored within the DR. The DR can resonate in various modes which are governed by the dimensions, geometry, and electrical properties of the DR itself and by the physical environment in which it is to operate. The development of temperature-stable high dielectric constant dielectric materials means that it is now possible to construct resonators which exhibit minimum change in resonant frequency with temperature.

The most commonly used DR shape is a solid cylinder. Here the most common mode of operation is denoted the $TE_{01\delta}$ or dipole mode, Fig. 3.

For a dielectric constant of 40 only 5% of the electric field and 40% of the magnetic field exist outside the DR. This energy decays rapidly as the distance from the DR surface increases (17). The resonant frequency of an isolated cyclindrical DR is given approximately by (18) as

$$f_{\mathrm{GHz}} = \frac{34}{a\sqrt{\epsilon_r}}\left[\frac{a}{\ell} + 3.45\right] \tag{1}$$

a, ℓ are in millimeters and $0.5 < a/\ell < 2$, while $30 < \epsilon_r < 50$.

For operation in fundamental mode the dimensions of the DR are approximately one guide wavelength; $\lambda g = \lambda_0/\sqrt{\epsilon_r}$.

The lowest frequency of operation is limited by tolerable DR size; typically this is 1 GHz, while the highest frequency, about 100 GHz, is governed by internal losses and minimum resonator dimensions (19). In order to avoid spurious modes

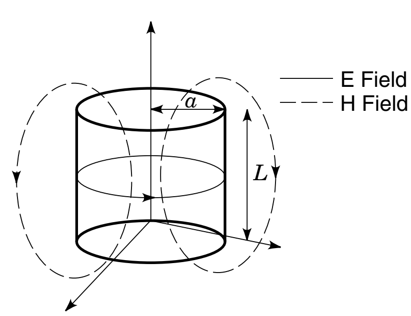

Figure 3. Cylindrical dielectric resonator $T_{01\delta}$ mode.

the length of the DR is usually restricted to lie between $0.175a \leq \ell \leq 0.225a$.

DIELECTRIC RESONATOR MATERIAL PROPERTIES

The Q-factor and temperature stability provided by dielectric resonators is invariably impaired by imperfect material parameters. The material from which the resonator is constructed will have losses produced by its finite conductivity and also by polarization induced damping under radio frequency (RF) excitation conditions (20).

If dielectric loss within the resonator is denoted, Q_d, then

$$Q_d = \frac{W}{W_d \tan\delta} \tag{2}$$

where $\tan\delta$ is the loss tangent of the resonator material. W is the total energy stored in the cavity and W_d is the energy stored in the dielectric resonator. Q_d is often quoted as

$$Q_d = \frac{C}{f} \tag{3}$$

where C is a constant quoted by the resonator manufacturer.

Sometimes the loss tangent is given as

$$\tan\delta = A + Bf \tag{4}$$

where A and B are constants quoted by the manufacturer.

A more complete description of the losses in the resonator yields the total dissipated power in the resonator P_{tot} to be:

$$P_{tot} = P_d + P_c + P_r + P_{ext} \tag{5}$$

where:

P_d = power dissipated in the dielectric material
P_c = power dissipated in the surrounding enclosed metal
P_r = radiation loss
P_{ext} = power coupled to the external circuit

From this, Q-factors for each term can be related to:

dielectric loss

$$Q_d = \frac{\omega W_e}{P_d} \tag{6}$$

conductor loss

$$Q_c = \frac{\omega W_e}{P_c} \tag{7}$$

radiation loss

$$Q_r = \frac{\omega W_e}{P_r} \tag{8}$$

external Q-factor

$$Q_{ext} = \frac{\omega W_e}{P_{ext}} \tag{9}$$

W_e is the total electric energy stored in the cavity defined by the shield enclosing the dielectric resonator.

The total loaded Q-factor for the enclosed DR is

$$\frac{1}{Q_L} = \frac{1}{Q_d} + \frac{1}{Q_c} + \frac{1}{Q_r} + \frac{1}{Q_{ext}} \tag{10}$$

while the unloaded Q-factor is

$$\frac{1}{Q_u} = \frac{1}{Q_d} + \frac{1}{Q_c} + \frac{1}{Q_r} \tag{11}$$

Techniques for measuring these quantities have been suggested in Refs. 21–23.

Temperature dependent effects which cause a change in the DRs stabilizing function within an oscillator also need to be quantified.

The linear coefficient of expansion for a material is defined as the change in length of a rod of the material $\Delta\ell$, divided by its length L such that

$$\frac{\Delta\ell}{L} = \alpha T \tag{12}$$

where α (ppm/°C) is the linear expansion coefficient. As a DR puck expands or contracts its resonant frequency will vary such that

$$\frac{\Delta f}{f_o} = -\alpha\Delta T \tag{13}$$

The negative sign indicates that as the DR puck becomes longer its resonant frequency decreases.

With a DR its relative permittivity, ϵ_r, is also a function of temperature. This variation is expressed very approximately as

$$\frac{\Delta\epsilon_r}{\epsilon_r} = \tau_E\Delta T \tag{14}$$

where τ_E is the temperature coefficient of the dielectric resonator (ppm/°C).

By combining these relationships together we obtain an approximate equation for the temperature stability of a DR

$$\frac{\Delta f}{f} = \frac{\partial f}{\partial L}\frac{\Delta L}{f} + \frac{\partial f}{\partial\epsilon_r}\frac{\Delta\epsilon_r}{f} \tag{15}$$

By denoting the temperature coefficient of the resonant frequency of the DR as τ_{DR} then:

$$\tau_{DR} = -\alpha - \frac{T_\epsilon}{2} \tag{16}$$

This equation implies that by making τ have twice the magnitude of α and giving it an opposite sense of operation that τ_ϵ can be reduced to zero, i.e., the DR can be temperature compensated. Note however since the DR will expand as temperature is increased τ must always be negative for temperature compensation to occur.

Consider now the effect these temperature changes have on the stability of a DRO. If an unstabilized oscillator has a negative frequency drift with temperature then a DR with a positive temperature coefficient is required so that temperature frequency stabilization can be achieved. The frequency stability τ_f of a DRO has been modeled in Ref. 24 as

$$\tau_f = \tau_{DR} + \left(\frac{k+2}{4Q_u}\right)\frac{\partial\phi}{\partial\tau} \tag{17}$$

where: $\partial\phi/\partial\tau$ is the temperature induced phase variation of the active circuit one port

$$\tau_{DR} = \frac{1}{f_o}\frac{df_o}{dT}$$

The second term just stated indicates that for a free running oscillator the frequency drift is amplified by an amount proportional to the coupling coefficient of the DR.

By arranging Eq. (17) it is possible to find the desired value for τ_{DR} which yields zero τ_f

$$\tau_{DR} = -\left(\frac{k+2}{4Q_u}\right)\frac{\partial\phi}{\partial\tau} \tag{18}$$

Here $\partial\phi/\partial\tau$ and τ_{DR} are unknown. The in-situ value for τ_{DR} when placed in its operating configuration can be found using a load pull technique.

Alternatively if $\partial\phi/\partial\tau$ is assumed to be constant for a small change in coupling coefficient k, then Eq. (17) can be used to form two simultaneous equations from which the in-situ τ_{DR} can be directly obtained. This second method should be used with caution since $\partial\phi/\partial\tau$ is nonlinear.

From this discussion it is clear that judicious selection of τ_{DR} and coupling coefficient can be used to compensate for temperature induced DRO frequency drift (24).

QUALITY FACTOR

Quality or Q factor relates energy stored to average power loss. In a DR based circuit, this is of critical importance since it is a measure of the resonator bandwidth, which is inversely proportional to Q factor. Temperature stability and AM/FM noise performance of dielectric resonator oscillator circuits also depend on the Q factor.

$$Q = \omega_0 \frac{\text{energy stored}}{\text{average power loss}} \tag{19}$$
$$\omega_0 = \text{resonant frequency rad/s}$$

A second equation for quality factor which relates to group delay through a resonant circuit is useful for oscillator work (25). This is the loaded quality factor, Q_L

$$Q_L = \omega_0\frac{\tau}{2} = -\frac{\omega_0}{720}\frac{d\phi}{df} \tag{20}$$

Here,

τ = group delay(s)
ϕ = phase of the open loop voltage transfer function (degrees).

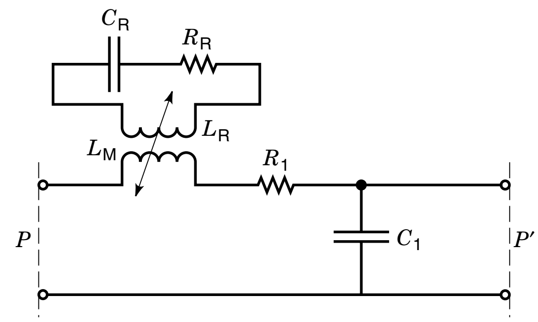

Figure 4. Equivalent circuit of DR coupled to microstrip line.

The loaded Q is used in oscillator design to express the width of the phase slope and resonance curve, including the effects of external components. As a consequence Q_L is dominated by components external to the DR which have their own Q factor, called, Q_{ext}.

The unloaded Q-factor, Q_u, is used when the Q of the resonant circuit is determined only by dissipation losses in the resonator. These various Q-factors are related as follows

$$\frac{1}{Q_L} = \frac{1}{Q_u} + \frac{1}{Q_{ext}} \tag{21}$$

For oscillator design Q_L can be used in the determination of single sideband noise prediction.

LUMPED ELEMENT COUPLING MODELS

By assuming that the aspect ratio of the DR and the frequency of operation have been selected such that only a single mode is excited then an isolated DR can be represented as a series resonant circuit with equivalent circuit components R_r, C_r, and L_r (26).

Figure 4 shows a DR coupled to a short section of microstrip line, at reference plane pp^1, which is represented by R_1, C_1, and L_1. When the resonator is excited in $T_{o1\delta}$ mode the coupling can be represented by a mutual inductance term L_m, which is proportional to the separation distance d, between the microstrip line and the DR, Fig. 4 (27).

If the microstrip line is assumed to have zero loss in the coupling region, R_1 can be neglected. By neglecting the microstrip line capacitance the resulting simplified equivalent circuit can be expressed close to resonance as a parallel resonant circuit Fig. 5.

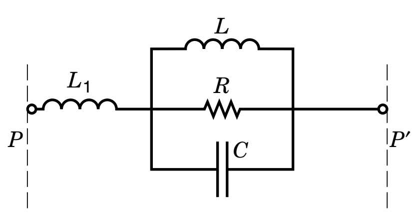

Figure 5. Simplified model of DR coupled to microstrip line.

where (28),

$$R = \frac{\omega^2 L_{\mathrm{m}}^2}{R_{\mathrm{r}}}$$
$$c = \frac{L_{\mathrm{r}}}{\omega^2 L_{\mathrm{m}}^2}$$
$$L = \omega^2 L_{\mathrm{m}}^2 C_{\mathrm{r}}$$

The general expression for a parallel resonant circuit is

$$Z = \frac{R}{1 + j2Q_0\delta} \tag{22}$$

Hence

$$Q_{\mathrm{u}} = \frac{\omega_0 L_{\mathrm{r}}}{R_{\mathrm{r}}} = \omega_0 RC \tag{23}$$

$$\omega_0^2 = \frac{1}{L_{\mathrm{r}} C_{\mathrm{r}}} = \frac{1}{LC} \tag{24}$$

$$\delta = \frac{\omega - \omega_0}{\omega} \tag{25}$$

Thus the equivalent circuit impedance, Fig. 4, can be written as

$$Z_{\mathrm{T}} = j\omega L_1 + \frac{R}{1 + j2Q_{\mathrm{u}}\delta} \tag{26}$$

These results are valid close to the fundamental resonance $TE_{\mathrm{o}1\delta}$ mode of the DR where δ^2 tends to zero. Outside this frequency range other DR modes exist, which can be modeled by a Foster-type equivalent circuit consisting of a series cascade of parallel tuned circuits (29). With this approach characterization of the ith resonant circuit requires the ith resonant frequency, unloaded Q-factor, and effective coupled resistance to be determined. In addition, when the resonant frequencies of several modes occur in close proximity the individual modal performances cannot be easily established due to mode interaction (30,31). It is useful to note that the $TE_{\mathrm{o}1\delta}$ mode can be well separated from other modes by correct selection of DR and enclosure dimensions.

When integrating the DR into an oscillator by means of a microstrip connecting line, the parallel tuned circuit in Fig. 5 becomes externally loaded as in Fig. 6.

Here the DR is loaded by the internal impedance of the generator and the load. If Z_{g} and Z_{L} are assumed to be real with line lengths ℓ_1 and ℓ_2 reduced to zero at resonance the parallel structure reduces to R. From Eq. (27) the value of R depends on the amount of coupling between the DR and the line. A coupling coefficient term observed at the input port is defined as the ratio of the resonator coupled resistance k at the resonator frequency to the resistance external to the resonator (32)

$$k = \frac{R}{R_{\mathrm{ex}}} \tag{27}$$

or

$$k = \frac{Q_{\mathrm{u}}}{Q_{\mathrm{e}}} \tag{28}$$

for a DR coupled to a matched line $R_{\mathrm{g}} = R_{\mathrm{L}} = Z_0$, here

$$k = \frac{R}{2Z_0} \tag{29}$$

for a DR coupled to a shorted load $R_{\mathrm{L}} = 0$, here

$$k = \frac{R}{Z_0} \tag{30}$$

When a reactive termination loads the resonant circuit this presents itself in series with the parallel equivalent circuit. This will cause an imperfect match and will cause an additional reactive load to appear in series with the equivalent circuit (33).

If x_1 is the normalized reactance appearing in series with the parallel resonant circuit then the definition for coupling coefficient observed at the input port becomes

$$k = \frac{R}{Z_{\mathrm{N}}(1 + x_1^2)} \tag{31}$$

and for a short circuit

$$k = \frac{R}{Z_0(1 + x_1^2)} \tag{32}$$

here

$$x_1 = \frac{\omega L_1}{Z_{\mathrm{N}}} \tag{33}$$

Z_{N} is the total impedance loading the DR.

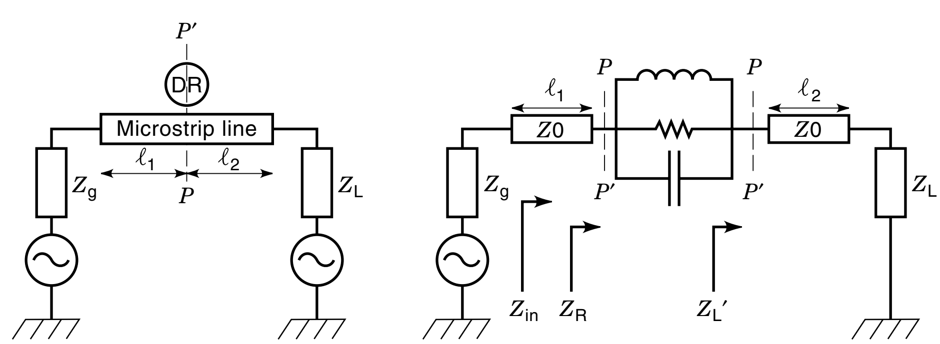

Figure 6. Oscillator DR coupling.

Also under these conditions the resonant frequency shifts to a new frequency f_L where:

$$f_L = f_0\left[1 + \frac{x_1 k}{2Q_u}\right] \tag{34}$$

and

$$Q_u = Q_L(1 + k) \tag{35}$$

When coupled to a matched microstrip line, x_1 is usually much less than one.

When the microstrip line lengths l_1, l_2 are not equal to zero, then the DR is coupled to the generator and load terminations Z_L, Z_g via microstrip line segments, ℓ_1, ℓ_2, Fig. 6.

For a matched line Eq. (28) is valid. For a short-circuit load and assuming lossless line

$$k = \frac{R}{Z_0(1 + \tan^2(\beta\ell_2))} \tag{36}$$

Here maximum coupling occurs at

$$\ell_2 = \frac{n\lambda_g}{4} \quad n = 0, 2, 4, \tag{37}$$

while minimum coupling occurs at

$$\ell_2 = \frac{m\lambda_g}{4} \quad m = 1, 3, 5, \tag{38}$$

where: λ_g = effective wavelength of the microstrip line.

The same result occurs when considering the impedance presented at the input port under similar conditions.

Terminating the line in an arbitrary reactance shifts the maxima and minima of the magnetic field along the line. Since the $TE_{01\delta}$ mode couples to the magnetic field, line coupling will be maximized at peaks in the magnetic field standing wave and minimized at troughs. Coupling to the maximum point on the standing wave will present the coupling coefficient given by the equation (29) at n = 0, 2, 4 . . . and so on. Maximum coupling coefficient is reported experimentally to consistently occur at a distance d = 0.7a, where a is the radius of the DR puck (33).

MEASUREMENT OF DR COUPLING COEFFICIENT

The most convenient method for experimentally estimating coupling coefficient k involves a measurement of loaded quality factor Q_L which is related to k as:

$$Q_L = \frac{Q_u}{1 + k} \tag{39}$$

However Q_u is not normally known and has to be determined by the losses at ω_0. From (34,35) Q_L can be established from the phase of the input impedance locus obtained by a one-port measurement made on the DR:

$$Q_L = \frac{f_0}{f_4 - f_3} \tag{40}$$

where f_0 is the center frequency; f_3 is the frequency at which the phase is lagging that at f_0 by 45°; and f_4 is the frequency at which the phase is leading that at f_0 by 45°. The results obtained by this method are typically 10% greater than those obtained by the method of deembedded S-parameters shown next.

By assuming zero radiation loss at the DR microstrip junction it can be shown from scattering parameter theory that for a matched system

$$k = \frac{1 - [S_{11}]^2 - [S_{21}]^2}{2[S_{21}]^2} \tag{41}$$

A number of useful computer source codes for computing the resonant frequency and unloaded Q-factor for shielded DRs are given in Ref. 36.

DIELECTRIC RESONATOR COUPLED TO A MICROSTRIP LINE

The most frequently used method of integrating a DR into a microwave integrated circuit is to couple it to a microstrip line. Here the problem is confined to the $TE_{01\delta}$ mode of a cylindrical DR, Fig. 1. Here the suffixes refer to the standing wave pattern in the azimuthal, radial, and axial directions respectively for the fundamental TE mode δ = 1.

A typical coupling configuration is shown in Fig. 7. An approximate representation of the H-field lines is given in order to illustrate the inductive nature of the coupling between a DR in $TE_{01\delta}$ mode and the quasi-TEM mode of microstrip line.

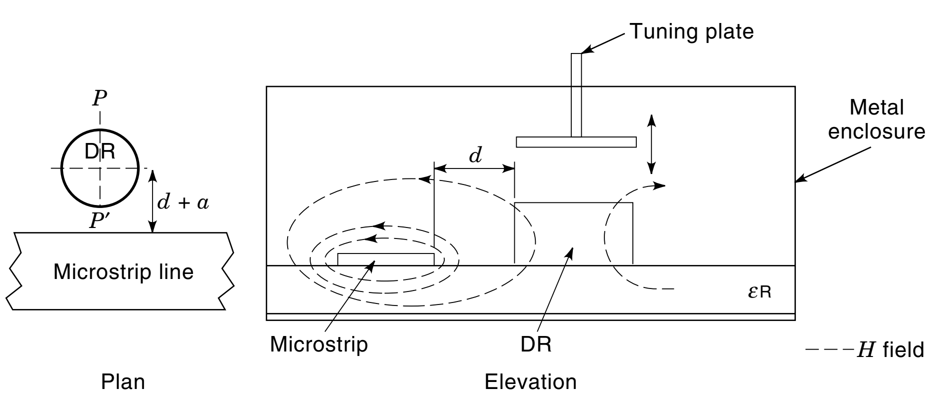

Figure 7. DR coupled to microstrip line, physical and electrical equivalent.

Here the magnetic field lines match each other principally on the radial direction of the DR field directly under the microstrip line. The coupling between the DR and the line is inversely proportional to the separation and, between them, is defined by a mutual inductance coupling coefficient term, k. With this type of coupling a proportion of energy is radiated away from the DR. Therefore the effect of losses in the microstrip substrate, signal line, and enclosure act to perturb the electromagnetic field and alter the Q-factor of the DR (37,38). For oscillator design an equivalent circuit model for the line DR coupled arrangement is required. The DR may be fixed to the line using a low-loss adhesive (39,40). If the adhesive has a slow setting time then reworking of the DR position for tuning can be made.

DIELECTRIC RESONATOR TUNING

For optimum phase noise designs the oscillator center frequency should be equal to that of the dielectric resonator. For many circuits it is useful to have a DR tuning facility. One way of achieving this is to use mechanical tuning, Fig. 8.

Here a metal (41), dielectric (42), or DR (43) plunger is inserted in either the top wall or the side wall of the structure. The presence of the tuning element causes a localized distortion of the electromagnetic fields. With a metal plunger the additional losses in the plunger lower the Q_u of the resonator as the coupling between DR and plunger becomes tighter, i.e., as L is reduced. For a metal plunger as L is reduced the frequency of operation is increased while the reverse is true for a dielectric plunger. Generally a DRO used with the metal plunger tuning arrangement also produces a reduced output power as L decreases. With this arrangement about a 3% tuning range can be made.

With a second DR replacing the plunger top-cap in Fig. 8 the resultant change in Q_u is smaller than for the metal tuner case. This arrangement yields about an 8% tuning range.

Electronic tuning of the DR is also possible using a varactor diode as the tuning element. This can be mounted internally to the DR (44) or more usually as the termination on a line coupled to the DR, Fig. 1. A large tuning range requires tight coupling between the DR and the varactor, which inevitably leads to a reduction in Q_u.

If Q_u is the unloaded Q of the varactor then (45)

$$Q_{u\tau} = \frac{Q_u}{2}\left(\frac{f_0}{\Delta f}\right) \tag{42}$$

where, $Q_{u\tau}$ is the unloaded Q of the varactor tuned DR and Δf is the change in resonance frequency.

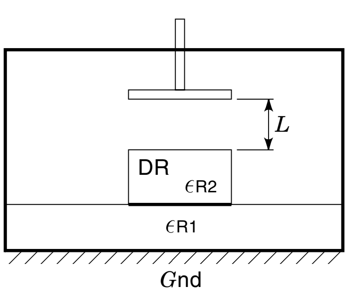

Figure 8. Mechanical DR tuning arrangement.

According to Ref. 45 about a 0.5% tuning bandwidth can be obtained with this arrangement.

Other techniques such as optical tuning (46), magnetic tuning (47), and segmented disk tuning also exist (48).

OSCILLATOR BASIC THEORY

Negative Resistance

In order for microwave oscillation to begin, a means to overcome the resistive losses in the circuit has to be provided. These losses include undesired stray and parasitic resistances, and also the load into which the oscillator must operate (usually 50Ω). To do this the concept of *negative resistance* is introduced. To illustrate the concept consider the simple equivalent circuit of Fig. 9. If the amount of negative resistance exactly cancels the sum of the positive resistances then the circuit will have a resonant or oscillation frequency where the inductive reactance is equal to the capacitive reactance. That is,

$$2\pi f L = \frac{1}{2\pi f C} \tag{43}$$

where f = resonant frequency, L = inductance, and C = capacitance. This condition is known as the *steady state oscillation condition.* In order for oscillation to buildup, an excess of negative resistance is required. Then, any small perturbation in the circuit, such as electrical noise, will kick-start a resonance. As oscillation builds the amount of negative resistance decreases until the steady state condition is met. A negative resistor can be formed from an unstable active device with suitable feedback applied. Consider a transistor with feedback such that the magnitude of the input reflection coefficient (S11) is greater than one. This means that when an ac signal is incident on the port, more energy is reflected than is actually incident. This can be regarded as a negative resistance.

Oscillator Equation

The 1-port negative resistance oscillator schematic is illustrated in Fig. 10. The oscillator can be considered as a 2-port negative resistance circuit and a 1-port resonator. The resulting oscillator then operates into a 1-port load. The large signal steady state oscillation condition is given by;

$$\Gamma_r.S11' = 1 \tag{44}$$

where Γ_r is the reflection coefficient of the resonator and S11′ is the large signal input reflection coefficient of the negative resistance circuit, when terminated in the load. The just

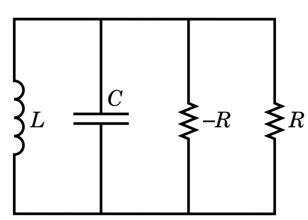

Figure 9. Simple equivalent circuit of a microwave oscillator.

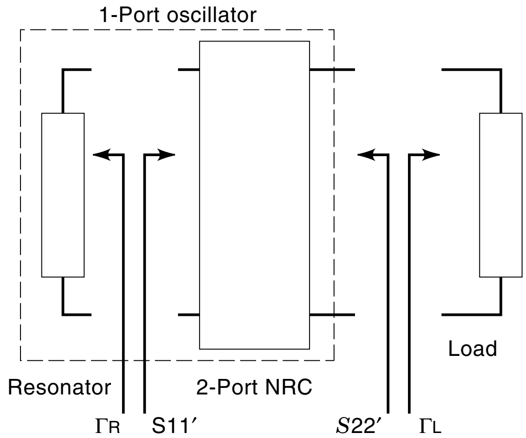

Figure 10. Negative resistance oscillator schematic showing port definitions.

stated reflection coefficients are complex numbers, and so the equation can be expanded into its magnitude and angle parts;

$$|\Gamma_r|.|S11'| = 1 \tag{45}$$

$$\mathrm{Ang}(\Gamma_r) + \mathrm{Ang}(S11') = 0 \tag{46}$$

If the equations are now expanded into impedance forms then we obtain

$$R + R_n = 0 \tag{47}$$

$$X_L + X_C = 0 \tag{48}$$

where R is the sum of positive resistances, R_n is the negative resistance, X_L is the inductive reactance, and X_C is the capacitive reactance. Equation (48) simply expands to Eq. (43) and determines the resonant frequency.

We have already stated that before steady-state oscillation can be achieved there must be an excess negative resistance to enable resonance to start. At the buildup of oscillation Eqs. (47) and (48) can be approximated to

$$r + r_n < 0 \tag{49}$$

$$x_L + x_C = 0 \tag{50}$$

where the resistances and reactances are now small-signal values. In terms of reflection coefficients the small-signal approximation to the oscillation condition becomes

$$|\Gamma_r|.|S11'| > 1 \tag{51}$$

$$\mathrm{Ang}(\Gamma_r) + \mathrm{Ang}(S11') = 0 \tag{52}$$

where the reflection coefficients are now the more easily measurable small-signal values. It should be noted here that Γ_r depends on the value of characteristic impedance Z_0 used to calculate it. Hence it is possible with this approach to find a startup condition in terms of Γ in one port but not in another for a given Z_0.

Oscillator Graphical Analysis

The solving of the small-signal *oscillation condition* is illustrated graphically in Fig. 11 with reference to Fig. 10. Here the Z (complex) represents the overall impedance of the closed loop oscillator, including the load. The frequency at which the imaginary part goes through zero (that is, resonance) is clear, and at this frequency there is an excess negative resistance.

N-port Oscillation Condition

It can be shown that the condition for oscillation is also present at the output port of the previously discussed negative resistance circuit. This means we could also solve

$$\Gamma_L \cdot S22' = 1 \tag{53}$$

where Γ_L is the reflection coefficient of the load and S22′ is the large signal output reflection coefficient of the negative resistance circuit, when terminated in the resonator. This condition can be shown to hold at all ports of an N-port oscillator (49).

Oscillator Figures of Merit

Frequency Pulling. As the reflection coefficient of the load, Γ_L, forms a vital part of Eq. (53), and influences the input reflection coefficient S11′ in Eq. (44), it is obvious that any change in its phase will have an effect on the oscillation frequency. The change in oscillation frequency due to a change in the load reflection coefficient is known as *frequency pulling.* This is usually determined by first measuring the frequency of an oscillator into a load of known reflection coefficient (often −12 dB). The phase of the load is then varied from 0 to 360° by means of a phase shifter or sliding load. The maximum deviation from the nominal frequency is the pulling figure. Pulling can be greatly reduced by isolating the oscillator's output from the load. This is usually achieved by use of a buffer amplifier with high reverse isolation.

Frequency Pushing. The basic function of the DRO is to convert dc energy to RF. The scattering parameters of the active device are dependent on the applied bias voltages and currents. Even regulated power supply voltages can experience fluctuations which lead to minute changes in output fre-

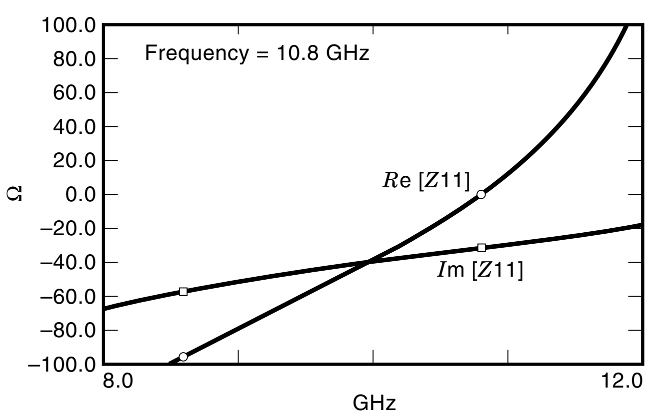

Figure 11. Graphical oscillator solution showing one-port oscillation condition.

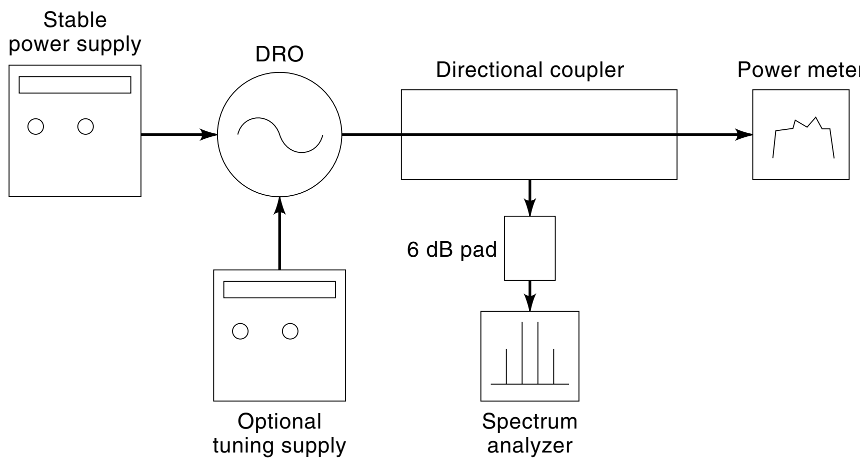

Figure 12. Typical DRO Test Set-Up for measuring power output and frequency spectrum.

quency. The change in oscillation frequency with respect to the dc supply voltage is known as *frequency pushing.* The parameter is measured by first noting the nominal oscillator frequency. The applied dc supply voltage is then varied (by one volt, for example) and the frequency deviation measured. Frequency pushing is then expressed in units of frequency per volt. In practical circuits pushing is minimized by using well regulated supply voltages.

Oscillator Stability

An oscillator is said to be stable if the output frequency (and power) do not vary with temperature and time. Dielectric resonators are good for producing stable oscillators because of their high Q-factors. Dielectric resonators may be used in oscillators in two distinct ways

1. As a high-Q passive element coupled to a free running oscillator. Here the DR is not used as the oscillator's main resonator, but is "locked" to this resonance. Such an oscillator is known as a *dielectrically stabilized oscillator* or DSO.
2. As a circuit element in the oscillator, whereby the DR actually determines the oscillation frequency.

It is known that free-running oscillators generally have a negative temperature coefficient. Thus the oscillator's frequency falls as temperature is increased. The temperature coefficient of a DR can be made positive by careful choice of material composition. Thus the DR can be made to compensate for free-running oscillator drift. The temperature stability of a complete DRO is dependent on (50)

- The coupling coefficient between the DR and the rest of the circuit
- The Q of the oscillator
- The rate of change of the active device's reflection coefficient phase with temperature

Typical variations in oscillator frequency with temperature in DROs are of the order of 4 ppm/°C. This value can be reduced, to values as low as 1 ppm/°C, by several techniques, including

- *Phase Locking.* A high frequency voltage controllable DRO is phase locked to a low frequency crystal oscillator of superior phase noise and stability; this improves long-term frequency stability.
- *Digital Compensation.* Here the performance of an oscillator with temperature is measured, and the information stored in programmable read-only memory. A temperature sensor circuit is then used, in conjunction with a look-up table, to apply a correction voltage to the oscillator in order to hold it at constant frequency.
- By stabilizing the DRO in a temperature-controlled localized oven (51).

The primary properties of a dielectric resonator oscillator, that is, frequency and output power, can be measured using the test set-up illustrated in Fig. 12. The frequency of oscillation is measured on a high frequency spectrum analyzer, or RF counter. The power can also be read from the analyzer display, but is often more accurately determined using a separate RF power meter.

Frequency pushing can now be determined by observing the shift in oscillation frequency as the supply voltage is varied. Pulling is measured by replacing the power meter with a tunable load of known return loss (usually 12dB). The phase of this load is then varied through 360°, and the resulting maximum excursion from the nominal frequency noted.

Phase noise can be measured on the analyzer display at suitable offset frequencies. A correction has to be made for the filter (resolution) bandwidth of the measuring instrument. More accurate phase noise measurement (especially close to the carrier) requires a dedicated phase noise test-set.

The above oscillator parameters are usually determined over a range of temperatures. This enables the variation of the frequency and output power with temperature to be determined.

OSCILLATOR PHASE NOISE

The phase noise of an oscillator is an important quantity. Ultimately phase noise limits adjacent channel selectivity in a receiver. The output signal from a physical oscillator is not monochromatic. In a real oscillator, noise sidebands arise since the frequency of the signal can vary with time due to phase noise created by phase modulation of the signal (52). The usual method for characterizing the noise is to determine the single-sideband (SSB) phase noise power spectral density at a given frequency offset from the carrier (dBc/Hz). A frequency offset figure of 10 kHz is often quoted.

The phase noise comes from the various noise sources available in the circuit as well as the active device intrinsic noise sources. These noise sources induce phase noise by nonlinear device mechanisms causing upconversion of the baseband noise to the oscillator frequency. Noise sources which are due to white noise generally contribute $1/f^2$ to the spectrum of the phase noise, while $1/f$ noise adds $1/f^3$ to the phase-noise spectrum. Individual noise sources are to a first approximation considered uncorrelated. In practice up and down conversion can occur leading to correlated amplitude modulated (AM) and frequency modulated (FM) noise effects. The $1/f$ noise acts to alter the frequency of the oscillation.

When designing a DRO with low phase noise the unloaded Q-factor of the resonator should be as high as possible. The $1/f$ noise of the active device should be as low as possible. JFETS then bipolar transistors and HBTs have the lowest $1/f$ noise with GaAs FETs having the worst $1/f$ performance. Also it is usual that the center frequency of oscillation of the DR should be equal to that of the oscillator. Here the DR acts to select the frequency of oscillation. Under these conditions the center frequency of the DR will have maximum rate of change of phase with respect to frequency, that is, the resonator will have its highest Q. Noise power density is split between AM and PM noise by equal amounts. In addition AM noise is usually much more dominant than PM noise at offset frequencies far removed from the carrier (53). Close to the carrier PM noise is the dominant factor. Methods for simulating oscillator phase noise are given in (54,55).

Leeson's Eq. (52) and Eq. (54) describe the expected single sideband (SSB) phase noise power density at a frequency f_m offset from the carrier for an oscillator using a single resonator; here:

$$L_{pm} \approx 10\log_{10}\left[\frac{NRkT}{A}\frac{1}{8Q_L^2}\left(\frac{f_0}{f_m}\right)^2\right] \text{ dBc/Hz} \tag{54}$$

where NR is the device noise ratio; A = oscillator output power; Q_L = loaded Q; f_0 = oscillator center frequency (Hz); and f_m = carrier offset (Hz).

Equation (54) shows that the oscillator SSB phase noise is affected by the loaded Q squared, i.e., 6 dB improvement per Q_L doubling, hence the incentive for using a DR with as high a Q as possible. Leeson's equation shows that the SSB phase noise reduces at 6 dB/octave over the range it applies. This range is for f_m greater than frequency f_1, the $1/f$ flicker noise corner frequency and less than below the frequency f_2 where $f_2 = f_o/2Q_L$. Above f_2 the oscillator upconverted white noise dominates. To correctly apply this equation the $1/f$ noise for the device must be known a priori. In addition the device noise ratio at its operating power level (assumed to be in the linear range of operation) and loaded Q for the circuit are also required. A detailed discussion of low noise oscillator design and measurement methods can be found in Ref. 56.

DESIGN EXAMPLE—10.8 GHz DRO

Consider the schematic of Fig. 13. The circuit consists of a common-source MESFET-based negative resistance circuit

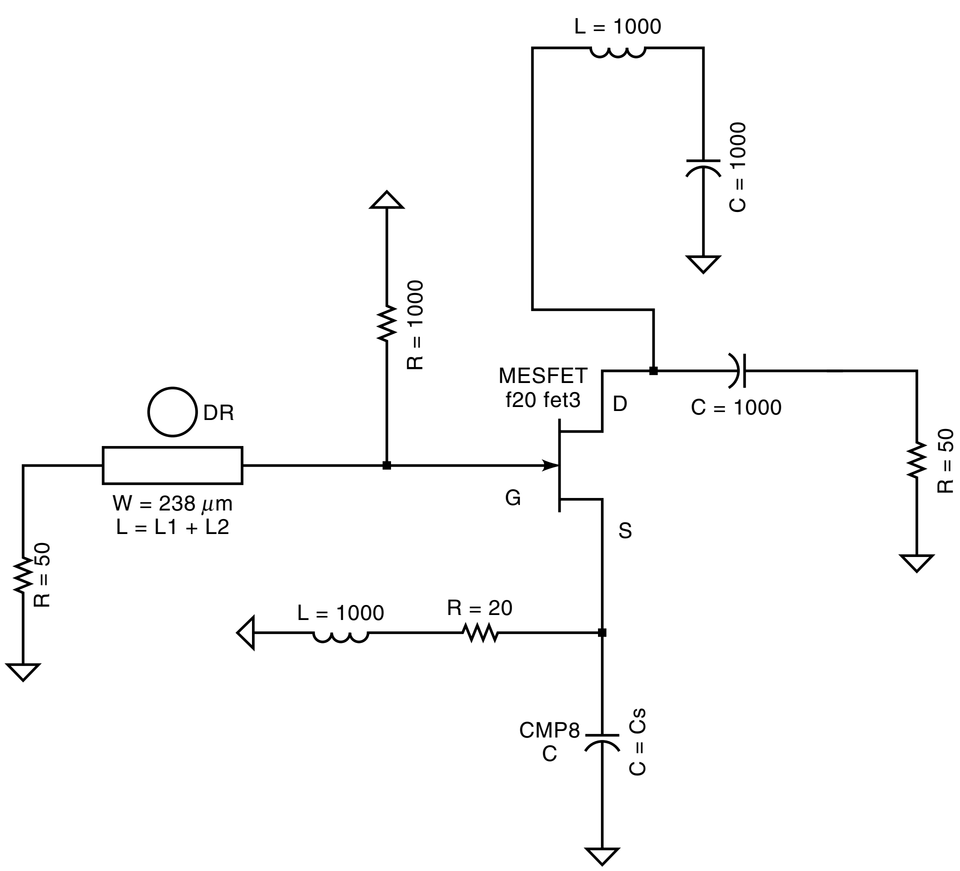

Figure 13. Circuit schematic for 10.8 GHz DRO example design (ϵ_r = 10.0, h = 254 μm).

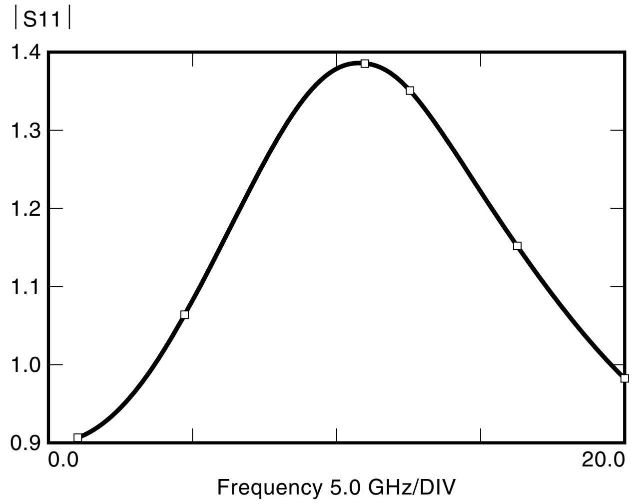

Figure 14. One-port input reflection plot.

(NRC), with series capacitive feedback. The DR is coupled to the gate via a 50 Ω terminated microstrip transmission line. The substrate for the transmission line is chosen to be 254 μm thick alumina (ϵ_r = 9.9). The width of the line is 238 μm which corresponds to a characteristic impedance of 50 Ω.

The first step is to choose a suitable DR size. As a practical example consider the Murata $TE_{01\delta}$ DRD series (57). The most suitable dimensions for a 10.8 GHz circuit are a diameter of 6.5 mm and a thickness of 2.9 mm. It can be shown that this puck will resonate at approximately 10.34 GHz when enclosed in a well spaced metallic environment. In a practical circuit the resonator will operate at a higher frequency due to the presence of the thin substrate. The shift in frequency can be approximated by the analytical formula in Ref. 50. Final tuning to 10.89 Hz by use of a metal tuning screw can then be achieved.

Step two involves choice of a suitable transistor and bias condition. For this example a GMMT 0.5 μm gate length/300 μm gate width GaAs MESFET is used. When biased at +5 V Vds and Ids = 50% Idss the transistor exhibits some 12 dB of available gain at this frequency. This is more than adequate for this type of oscillator design.

Next the 2-port NRC is designed. To do this the series capacitive feedback is varied until the magnitude of the input reflection coefficient (S11) is greater than one, indicating negative resistance. In practice a value greater than 1.2 should be used. This is generally enough to ensure sufficient excess negative resistance to kick-start an oscillation. For this transistor a value of 0.24 pF results in |S11| being of the order of 1.4 at 11 GHz, as illustrated in Fig. 14.

Next the complete oscillator is simulated to solve the small-signal approximation to the complex condition for oscillation, that is, $\Gamma \cdot S11 > 1$. A model for the coupled DR can be developed using the mutually coupled parallel LCR model and coupling factor, k, as previously discussed. In practice the equivalent circuit is merely an RF open-circuit at resonance. Therefore the circuit can be simplified to the circuit shown in Fig. 15. To complete the oscillator design the transmission line length l_1, at which point the center of the DR is placed, is calculated. For this example a value of 4.427 mm is deter-

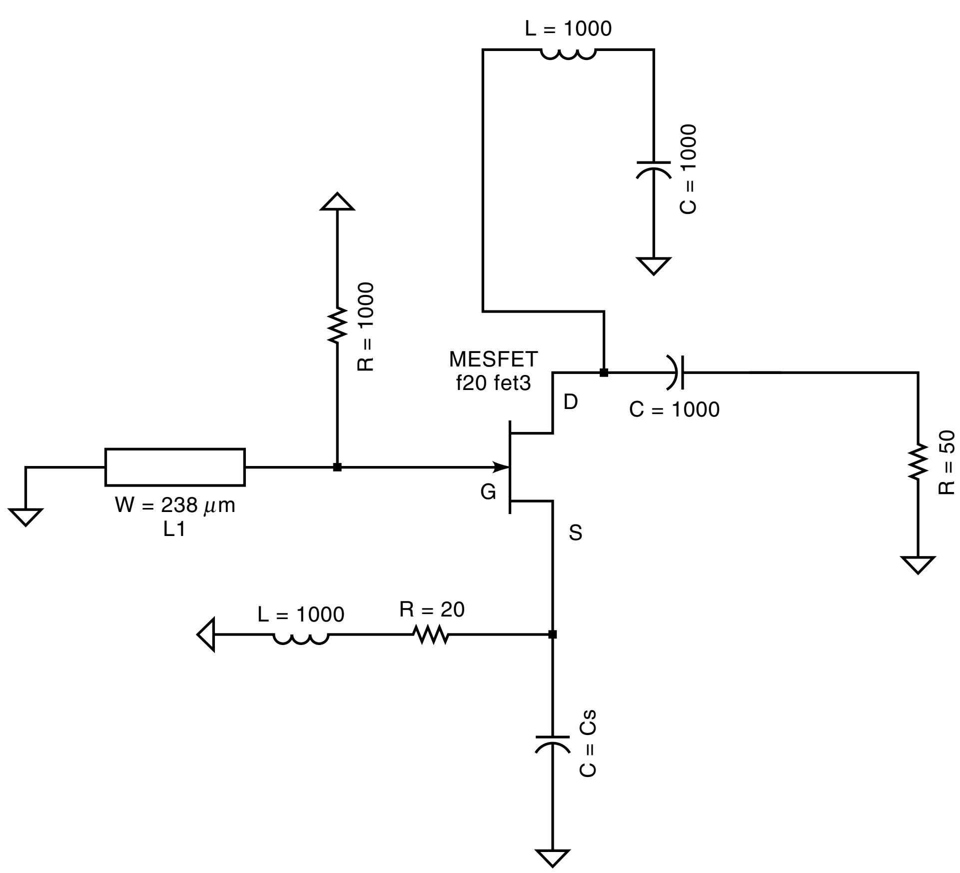

Figure 15. Simplified equivalent circuit for 10.8 GHz DRO example design.

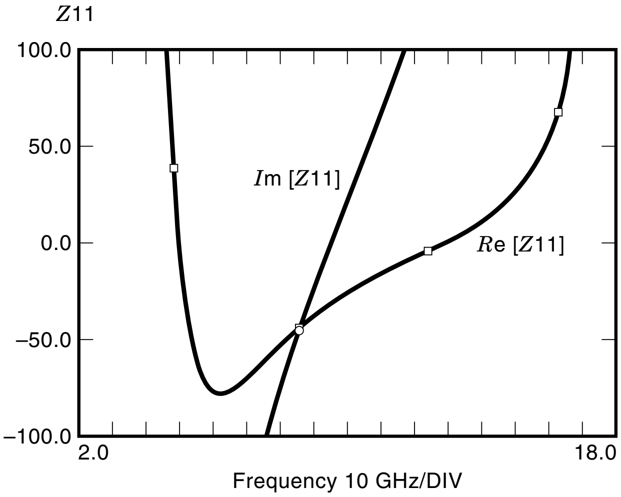

Figure 16. One-port oscillation condition.

mined. The resulting oscillation frequency, in terms of real and imaginary parts of the overall impedance, is shown in Fig. 16. The angle goes through zero at 10.8 GHz, with the resulting magnitude simultaneously being greater than 1.2. A large-signal simulation can be performed using a harmonic balance technique to predict output power and other important oscillator parameters. For this example +11 dBm output power was predicted, with a dc to RF conversion efficiency of approximately 13%. In addition the phase noise was predicted as −80 dBc/Hz at 10 kHz offset. This is achieved by including important noise parameter values in the nonlinear device model.

In practice the circuit is now fabricated by using an arbitrary length for l_2, and suitably terminating the line in the characteristic impedance, 50 Ω. The circuit is biased as required and the DR placed on the alumina in approximately the correct position. The puck is then moved around until oscillation of suitable magnitude, Q-factor and phase noise is obtained. The resonator is then fixed into position, and mechanically tuned to the exact required frequency.

Electronic tuning of the circuit to enable phase locking to a crystal reference is possible. To achieve this a $\lambda/4$ length of transmission line incorporating a tuning varactor is also coupled to the resonator. Tuning the varactor capacitance changes the phase of the coupled line, resulting in pulling of the DR frequency.

DRO CAD TECHNIQUES

The practical realization of dielectric resonator oscillators DROs can be assisted by the use of linear and nonlinear CAD tools. Linear scattering parameters can be used to represent the active device and feedback network (3,58–61). Important DRO performance features such as output power, efficiency, steady state stability and tuning range, have been simulated (62–64).

Series feedback DROs have been designed using S-parameter methods whereby a topology is selected to yield maximum negative resistance at one port while maintaining small-signal start-up conditions (50,65). When parallel feedback topology is used a more complex design procedure is required (66). Here, when the DR is coupled between two of the device terminals, the reflection coefficient at the third terminal Γ_3 is expressed in terms of the DR and active device scattering parameters. The position of the DR and hence the coupling coefficient are optimized to maximize Γ_3 and a matching circuit designed to maximize the start-up condition (61).

Small signal techniques do not necessarily lead to maximum power oscillators nor do they ensure stability of operation. Nonlinear large signal techniques are needed to do this. Broadly two classes exist here, time domain (67) and harmonic balance (68). The former method uses numerical integration of state space equations describing the active device and the embedding circuit. All circuit elements must be represented in the time variable as voltage dependent current equations. There are no constraints on the harmonic content, hence highly nonlinear circuits can be examined. The time domain approach is well suited to oscillator simulation because oscillation start-up, transient, and steady response can all be obtained on a single analysis run. However, each time step must be small enough to ensure numerical convergence of the integration routine. This is a severe limitation when high Q resonators such as DRs are used (69).

With the harmonic balance approach, nonlinear circuit elements are analyzed in the time domain and transformed into the frequency domain where they are represented by a finite number of harmonic currents. Linear elements are solved directly in the frequency domain. Where linear and nonlinear components are joined current continuity forms the boundary condition for the harmonic balance algorithm. With this approach the high Q circuits are solved by numerically efficient algorithms directly in the frequency domain. However, in order to simulate circuits with strong nonlinearities many harmonics are needed for accurate representation of the nonlinear waveforms, thus increasing computational time. In addition, the harmonic balance approach yields only steady-state information about the oscillators behavior.

In a DRO the DR dampens higher harmonics, thus the harmonic balance approach is attractive here (63). In (63) the device topology was fixed a priori and the circuit element values were numerically optimized to satisfy a prescribed set of electrical specifications. An alternative approach is to synthesize from the maximum added power condition the general device terminations (70). This approach has been adapted for DRO synthesis (71,72). Most commercially available industrial circuit simulators for microwave use such as (73) will handle time domain and harmonic balance simulation with embedded large-signal active device models.

BIBLIOGRAPHY

1. C. L. Ren and J. K. Ploude, Application of dielectric resonators in microwave components, *IEEE Trans. Microw. Theory Tech.*, **MTT-29**: 754–759, 1981.
2. S. J. Fiedziuszko, Microwave dielectric resonators, *Microw. J.*, September 1986, p. 189.
3. A. Khanna, Parallel feedback FET DRO using 3-port S-parameters, *IEEE Int. Microwave Symp. Dig.,* San Francisco, 1984, pp. 181–183.
4. H. Abe et al., A highly stabilized low-noise GaAs FET integrated oscillator with a dielectric resonator in the C-band, *IEEE Trans. Microwave Theory Tech.,* **MTT-26** (3): 156–162, 1978.

5. R. S. Pengelly, *Microwave FETs—Theory, Design and Applications,* 2nd ed., New York: Wiley, 1986.
6. O. Ishikora et al., A highly stabilized GaAs FET oscillator using a dielectric resonator feedback circuit in the 9–14 GHz range, *IEEE Trans. Microwave Theory Tech.,* **MTT-28** (8): 817–824, 1980.
7. K. W. Lee et al., Push-push, frequency doubling, *MMIC Oscillators, IEEE GaAs IC Symp.,* 1987, pp. 227–230.
8. S. Chen et al., U-Band MMIC HBT DRO, *IEEE Microwave Guided Wave Let.,* **4** (2): pp. 50–52, 1994.
9. K. Borst, N. Loechel, and K. Wacker, Low noise synthesized microwave local oscillator for high capacity digital radio systems using a dielectric resonator and a SAW reference, *19th European Microwave Conference,* London, 1989, pp. 555–560.
10. K. Imai and H. Nakakita, A 22 GHz band low noise down converter for satellite broadcast receivers, *19th European Microwave Conference,* London, 1989, pp. 549–554.
11. C. D. Prasad, S. S. Serin, and D. Singh, 35 GHz dielectric resonator stabilized gunn oscillator, *Int. J. Infrared Millimeter Waves,* **17** (2): 393–402, 1996.
12. K. Ogawa et al., 25 GHz dielectric resonator oscillator using an Al GaAs/GaAs HBT, *Electron. Lett.,* **26** (18): 1514–1516, 1990.
13. D. Cros and P. Guillon, Whispering Gallery dielectric resonator modes for W-band devices, *IEEE Microwave Theory Tech.,* **38** (11): 1036, 1990.
14. A. Bermadez et al., A 94 GHz low noise GaAs FET oscillator using whispering gallery dielectric resonator modes and a new push-push configuration reducing l/*f* converted noise, *IEEE MTT-S Int. Microwave Symp. Dig.,* 1988, pp. 481–484.
15. S. Kharkovsky, A. Kirichenko, and A. Kogut, Solid-state oscillators with whispering-gallery mode dielectric resonators, *Microwave Opt. Technol. Lett.,* **12** (4): 210–213, 1996.
16. I. U. Khairuddin and I. C. Hunter, Whispering-gallery dielectric resonator mode GaAs FET oscillator, *IEE Proc.—Microwaves, Antennas Propag.,* **143** (5): 441–443, 1996.
17. D. Kajfez, Simple models, in D. Kajfez and P. Guillon (eds.), *Dielectric Resonators,* Dedham, MA: Artech House, 1986.
18. A. W. Gisson, Integrated equation methods, in D. Kajfez and P. Guillon (eds.), *Dielectric Resonators,* Dedham, MA: Artech House, 1986.
19. M. R. Stieglitz, Dielectric resonators: Past, present and future, *Microwave J.,* pp. 121–126, April 1989.
20. R. E. Collin, *Foundations for Microwave Engineering,* New York: McGraw Hill, 1966, pp. 17–20.
21. B. W. Hakki and P. D. Coleman, A dielectric resonator method of measuring inductive capacities in the millimetre range, *IRE Trans. Microwave Theory Tech.,* **MTT-8**: 402–410, 1960.
22. W. E. Courtney, Analysis and evaluation of a method of measuring the complex permittivity and permeability of microwave insulators, *IEEE Trans. Microwave Theory Tech.,* **MTT-18**: 476–485, 1970.
23. C. Tsironis, Highly stable dielectric resonator FET oscillators, *IEEE Trans. Microwave Theory Tech.,* **MTT-33** (4): 1011–1025, 1985.
24. M. Massias, M. J. Howes, and V. Postoyalko, A novel analysis and design technique for temperature stable DRO's, *19th European Microwave Conference,* London, 1989, pp. 418–423.
25. K. Kurokawa, Microwave solid state oscillator circuits, in M. J. Howes and O. V. Morgan (eds.), *Microwave Devices—Device Circuit Interactions,* New York: Wiley, 1976.
26. R. R. Bonetti and A. E. Atia, Generalized dielectric resonator filters, *COMSAT Tech. Rev.,* **11** (2): 321–343, 1981.
27. P. Guillon and S. Mekerta, A bandstop dielectric resonator filter, *IEEE MTT-S Int. Microwave Symp. Dig.,* 1981, pp. 170–173.
28. B. Ginzton, *Microwave Measurements,* New York: McGraw Hill, 1957, pp. 391–427.
29. D. Kajfez and E. J. Hwan, *Q*-Factor measurement with a network analyser, *IEEE Trans. Microw. Theory Tech.,* **MTT-32** (7): 666–670, 1984.
30. T. Hammersley, J. Richardson, and V. Postoyalko, Varactor tuning of dielectric resonator oscillators, *Microwave Engineering Europe,* pp. 25–28, May/June 1990.
31. W. P. Wheless and D. Kajfez, Experimental characterization of multi-moded microwave resonators using an automated network analyser, *IEEE Trans. Microw. Theory Tech.,* **MTT-35** (12): 1263–1270, 1987.
32. A. Khanna and Y. Gorault, Determination of loaded, unloaded and external quality factors of a dielectric resonator coupled to a microstrip line, *IEEE Trans. Microw. Theory Tech.,* **MTT-31** (3): 261–264, 1983.
33. Alpha Industries, The tuning and exciting of DR modes, *Mickrowelter Mag.,* **11** (Part 6): 550–552, 1985.
34. B. Ginzton, *Microwave Measurements,* New York: McGraw Hill, 1957, pp. 391–427.
35. A. P. S. Khanna, Q measurement of microstrip coupled dielectric resonators, *Microwaves and RF,* **23** (1): 81–86, 1984.
36. L. A. Trinogga, G. Kaizhou, and F. C. Hunter, *Practical Microstrip Circuit Design,* Chichester, UK: Ellis Horwood, 1991.
37. P. Guillon, B. Bysery, and M. Chaubet, Coupling parameters between a dielectric resonator and a microstrip line, *IEEE Trans. Microw. Theory Tech.,* **MTT-33** (3): 222–226, 1985.
38. P. Guillon and Y. Garault, Coupling between a microstrip transmission line and a dielectric resonator, *IEEE MTT-S Int. Microwave Symp. Dig.,* 1976, pp. 200–202.
39. Trans-Bond, Trans-Tech., Inc., Dielectric Resonator Mounting Adhesive, Alpha Industries, 19/21 Chapel St., Marlow, Bucks, SL7 3HN, UK.
40. Araldite Epoxy Resin, Ciba-Geigy, Plastics, Duxford, Cambridge, CB2 4QA, UK.
41. D. Kajfez, Simple Models, in D. Kajfez and P. Guillon (eds.), *Dielectric Resonators,* Dedham, MA: Artech House, 1986.
42. Alpha Industries, *A Designer's Guide to Microwave Dielectric Ceramics,* Marlow, Bucks, UK: Trans-Tech, Inc., 1990, Publ. No. 5008040, Rev. 2.
43. K. Wada, E. Nagata, and I. Haga, Wideband tunable DR VCO, *Proc. 15th European Microwave Conference,* 1985, pp. 407–412.
44. L. A. Trinogga and A. J. Fox, Inclusive varactor tuning of dielectric resonator filters, *26th European Microwave Conference,* Prague, pp. 162–164, Sept., 1996.
45. O. Y. Chan and S. Kazeminejad, Voltage controlled oscillator using dielectric resonator, *Electron. Lett.,* **24** (13): 407–412, 1988.
46. P. R. Herczfeld and A. S. Daryoush, Optically tuned and FM modulated x-band dielectric resonator oscillator, *Proc. 14th European Microwave Conference,* Liege, Belgium, 1984, pp. 268–273.
47. J. Krupka, Magnetic tuning of cyclindrical Ho1δ-mode dielectric resonators, *IEEE Trans. Microwave Theory Tech.,* **MTT-37**: 743–747, 1989.
48. A. Nesic, A new method for frequency modulation of dielectric resonator oscillators, *Proc. 15th European Microwave Conference,* 1985, pp. 403–406.
49. K. Kurokawa, Microwave solid state oscillator circuits, in M. J. Howes and O. V. Morgan (eds.), *Microwave Devices—Device Circuit Interactions,* New York: Wiley, 1976.
50. D. Kajfez and P. Guillon (eds.), *Dielectric Resonators,* Dedham, MA: Artech House, 1986.
51. *Fundamentals of Quartz Oscillators,* Hewlett Packard Application Note 200-2, Electronic Counter Series, Santa Rosa, CA, 1980.
52. D. B. Leeson, A simple model of feedback oscillation noise spectrum (Letters), *Proc. IEEE,* February 1996, pp. 329–330.

53. S. Hamilton, FM and AM noise in microwave oscillators, *Microwave J.,* June 1978, pp. 105–109.
54. Hewlett-Packard, *Simulating Noise in Nonlinear Circuits using the HP Microwave and RF Design Systems,* Santa Rosa, CA, 1993, Product Note 85150-4.
55. A. Howard, Simulate oscillator phase noise, *Microwaves and RF,* November 1993, pp. 64–70.
56. G. D. Vendelin, *Design of Amplifiers and Oscillators by the S-parameter Method,* New York: Wiley, 1982, pp. 145–162.
57. Data Sheet, *Microwave Ceramic Resonator Catalogue,* Murata-Erie Publication, No. 58-04C, Tokyo, Japan, 1994.
58. K. Borst, N. Loechel, and K. Wacker, Low noise synthesized microwave local oscillator for high capacity digital radio systems using a dielectric resonator and a SAW reference, *19th European Microwave Conference,* London, 1989, pp. 555–560.
59. P. G. Wilson and R. D. Carver, An easy-to-use FET DRO design procedure suited to most CAD programs, *IEEE MTT-S Int. Microwave Symp. Dig.,* 1989, pp. 1033–1036.
60. C. Y. Ho and T. Kajiba, DRO state of the art, *Appl. Microwave,* Microwave Symposium Digest, Vol. 3, Long Beach, CA, Spring 1990.
61. A. C. Murphy and P. J. Murphy, Computer program aids dielectric resonator feedback oscillator design, *Microwave J.,* September 1988, p. 131.
62. A. M. Pavio and M. A. Smith, A 20-40 GHz push-push dielectric resonator oscillator, *IEEE Trans. Microw. Theory Tech.,* **MTT-33** (12), 1346–1349, 1985.
63. V. Rizzoli, A. Costanzo, and A. Neri, Analysis and optimization of DROs using a general-purpose CAD program, *Alta Freq.,* **57** (7): 389–398, 1988.
64. F. Filicori, V. A. Moncaco, and G. Vannini, A design method for parallel feedback dielectric oscillators, *19th European Microwave Conference,* London, 1989, pp. 412–417.
65. A. Sweet, *MIC and MMIC Amplifier and Oscillator Circuit Design,* Dedham, MA: Artech House, 1990.
66. A. Podocomeni and L. Conrodo, Design of microwave oscillators and filters using transmission mode dielectric resonators coupled to microstrip lines, *IEEE Trans. Microw. Theory Tech.,* **MTT-33**: 1324–1332, 1985.
67. M. I. Sobhy and A. K. Jastrezebski, Computer-aided design of microwave integrated circuits, *Proc. 14th European Microwave Conference,* Liege, Belgium, 1984, pp. 705–710.
68. V. Rizzoli, A. Lipperini, and E. Menazzi, A general purpose program for non-linear microwave circuit design, *IEEE Trans. Microw. Theory Tech.,* **MTT-31**: 762–770, 1983.
69. I. Kipinis and A. S. Khanna, Large signal computer-aided analysis and design of silicon bipolar MMIC oscillators and mixers, *IEEE Trans. Microw. Theory Tech.,* **MTT-37** (3): 558–564, 1989.
70. Y. Xuan and C. Snowden, A generalized approach to the design of microwave oscillators, *IEEE Trans. Microw. Theory Tech.,* **MTT-35** (12): 1340–1347, 1987.
71. S. W. J. Seawright et al., Optimum DRO synthesis, *19th European Microwave Conference,* London, 1989, pp. 406–411.
72. S. W. J. Seawright et al., Computer-aided design of a microwave MESFET DRO, *19th European Conference on Circuit Theory and Design,* 1989, pp. 561–565.
73. Hewlett-Packard, *Microwave and RF Design System,* MDS, Vols. 1–8, Brighton, England, 1989.

VINCENT F. FUSCO
Queen's University of Belfast

ANDREW DEARN
Plextek Ltd.

DIELECTRICS, GATE AND TUNNEL. See GATE AND TUNNEL DIELECTRICS, MANUFACTURING ASPECTS.

DIELECTRICS, PHOTOCONDUCTIVE. See PHOTOELECTRETS.

DIE PRODUCTS. See KNOWN GOOD DIE TECHNOLOGY.